metals

MDPI

Article

High-Precision Optical Excited Heaters Based on Au Nanoparticles and Water-Soluble Porphyrin

Alexey V. Povolotskiy [1,*], Oksana S. Smirnova [1], Diana A. Soldatova [1], Anastasia V. Povolotckaia [2] and Daniil A. Lukyanov [1]

[1] Institute of Chemistry, Saint-Petersburg State University, 199034 Saint-Petersburg, Russia
[2] Center for Optical and Laser Materials Research, Saint-Petersburg State University, 199034 Saint-Petersburg, Russia; anastasia.povolotckaia@spbu.ru
* Correspondence: alexey.povolotskiy@spbu.ru

Abstract: Gold nanoparticles are widely used as local heaters under optical excitation. Hybrid molecular-plasmon nanostructures based on gold nanoparticles and water-soluble porphyrin have been developed. A colloidal solution of gold nanoparticles was obtained by laser ablation of metallic gold in water, ensuring its highest chemical purity. The hybrid nanostructures formation was performed due to the Coulomb interaction of cationic porphyrin and gold nanoparticles. The revealed functional properties of hybrid nanostructures make them promising for controllable nano-heater applications (for example, photothermal therapy). Gold nanoparticles act as heaters, whereas porphyrin serves as a fluorescent thermometer with a single optical excitation.

Keywords: gold; hybrid nanoparticles; optical excitation; heater; porphyrin; ratiometric fluorescent thermometer; photothermal therapy

check for updates

Citation: Povolotskiy, A.V.; Smirnova, O.S.; Soldatova, D.A.; Povolotckaia, A.V.; Lukyanov, D.A. High-Precision Optical Excited Heaters Based on Au Nanoparticles and Water-Soluble Porphyrin. *Metals* **2023**, *13*, 1851. https://doi.org/10.3390/met13111851

Academic Editors: Zhongxia Shang and Jaehun Cho

Received: 26 September 2023
Revised: 25 October 2023
Accepted: 31 October 2023
Published: 5 November 2023

1. Introduction

Gold (Au) nanoparticles (NPs) are extremely promising as heaters under optical excitation in the plasmon absorption band [1–4]. Moreover, depending on the morphology, the broad plasmon absorption band can be shifted to the red region of the spectrum, therefore various laser sources could be used for excitation [5,6]. One of the recent studies in the field of plasma nanostructures is related to the system symmetry breaking [7]. However, spherical nanoparticles are more convenient from the point of view of predicting functional features, and therefore remain indispensable model samples for the research devoted to the plasmonic nanostructures interaction with molecular systems. In particular, Au NPs can be optically pumped by lasers with a wavelength corresponding to the transparency window of biological tissues [3].

To date, Au NPs possess chemical inertness and potential long-term biocompatibility making them promising objects in medicine [5]. The ability to vary the Au NPs size, shape, functionalization, and surface charge allows us to design structures with properties required for a particular application [8–10]. The hybrid molecular-plasmonic nanostructures creation, based on porphyrins and Au NPs, results in particles with unique properties that individual components do not possess [11,12]. Many works are devoted to the study of porphyrins [13–16]. Its chemical and optical properties, as well as wide distribution in nature, determine possible applications in various fields, from spintronics [17] and solar cell prototypes [18] to analytical chemistry and photomedicine [16,19,20]. One of the promising areas for the usage of porphyrin structures is the ratiometric fluorescent sensors formation, in particular, molecular thermometers for noninvasive temperature detection [21]. Fluorescent molecular thermometers, due to the required tissue overheating control to prevent the possible necrosis, could be an indispensable device for determining the temperature during photothermal therapy [22].

The photothermal therapy operation principle can be considered using the example of plasmonic NPs. After injection and intratumoral accumulation, plasmonic NPs are exposed to light of a certain wavelength in the near infrared (IR) range [23], leading to the appearance of a localized surface plasmon resonance and, as a consequence, the conversion of light into heat [22]. The absorption spectrum of a gold nanoparticles colloidal solution strongly depends on their diameter. The position of the plasmon absorption maximum shifts to the long-wavelength region with an increasing nanoparticle size: with a nanoparticle diameter of 9 nm, the maximum is in the region of 517 nm, and with a diameter of 99 nm, the corresponding band has a center at 575 nm [5]. Hyperthermia causes cell death through three mechanisms: destruction of the cell membrane, denaturation of tumor DNA, and angiogenesis block [24]. The cell death during photothermal therapy is highly dependent on the affected tissues' heating temperature. Thus, at 43 °C temperatures or below, most cells in the affected area survive, making therapy ineffective. When tissues heat up to 49 °C, the contribution of necrosis becomes too large, posing a danger to surrounding healthy cells. As a result, during photothermal therapy of oncological diseases in vivo, it is necessary to maintain the tissues temperature at the local exposure area in the 44–48 °C range, while the optimal ratio of apoptosis and necroptosis to necrosis and excess of surviving cells is observed at about 46 °C [25]. The basic method of temperature measurement in aforementioned studies is the temperature determination of the surrounding tissue and not the thermometer itself. The temperature of the heating elements—plasmonic NPs—is not controlled in any way, which results in the local tissue overheating in the vicinity of metal NPs, while the average tissue temperature remains within the normal range. Thus, in all the aforementioned works, a crucial characteristic, the heaters temperature, is missing, which might lead to incorrect interpretation of the observed data, including the temperature corresponding to a high probability of necrosis. The ability to accurately record the temperature of the heaters themselves and not only the temperature of tissues in the area of nanoparticles impact, is a fundamental task for the development of photothermal therapy. This work is devoted to the development of hybrid molecular-plasmon NPs based on porphyrins and Au NPs for use in photothermal therapy.

2. Materials and Methods

2.1. Synthesis of Gold Nanoparticles

The Au NPs synthesis was carried out by laser ablation in a liquid. Figure 1 shows the optical scheme of the experimental setup. The gold target (99.99%) was placed in a quartz cuvette with 25 mL of water using a holder mounted on a 2D motorized translator, assembled on the basis of two linear Standa translators. Deionized water was used for the synthesis, prepared using the Millipore Simplicity UV Water Purification System, resistance 18 MOhm/cm. Laser radiation was focused on the gold target surface using a lens with 10 cm focal distance. The Innolas Spitlight 2000 pulsed laser with a 1064 nm wavelength was used as the excitation source, with 1 J pulse energy, 10 Hz repetition rate and 7 ns pulse duration. During laser ablation, a motorized translator moves the target relative to the laser focal spot at a speed of 0.1 mm/s along the trajectory shown in the inset of Figure 1. Scanning the laser over the surface allows us to avoid the formation of craters and perform ablation from the entire surface of the target. As a result of irradiation (about 1–2 min), a colloidal solution of Au NPs with the characteristic pink color was formed.

The size distribution of the synthesized Au NPs and the measurement of the Zeta potential were carried out by dynamic light scattering using the particle size analyzer SZ100 (Horiba Scientific, Piscataway, NJ, USA). The SZ100 analyzer is equipped with a 532 nm 10 mW laser source. All measurements were carried out in a quartz cell at a 173° scattering angle. During the measurements, the refractive index of gold was set to 0.27, the viscosity of the solvent was set to 0.887 Pa, and the refractive index of the solution was set to 1.333.

SEM images of gold nanoparticles and EDX analysis were carried out using a Zeiss Merlin scanning electron microscope equipped with an Oxford Instruments INCAx-act energy-dispersive X-ray spectrometer.

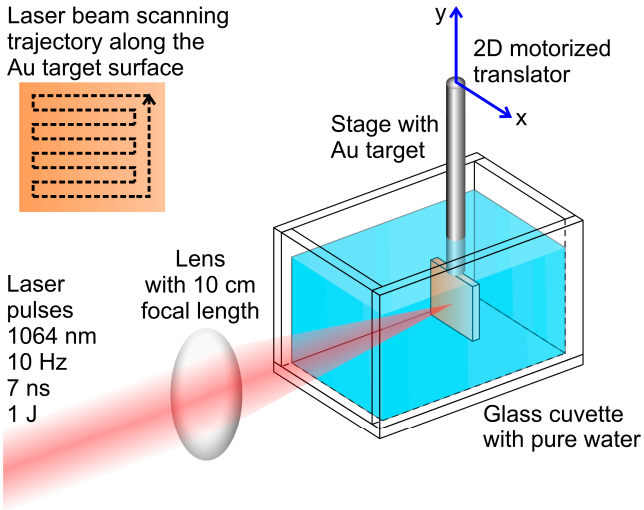

Figure 1. Optical scheme of experimental setup for Au NPs synthesis.

2.2. Synthesis of Porphyrin

Cationic porphyrin 4,4′,4″,4‴-(5,10,15,20-Porphyrintetrayl)tetrakis(1-methylpyridinium) 4-methylphenylsulfonate (TMPyP4+) in the form of p-toluenesulfonate (TMPyP-OTs) was prepared in two stages using literature procedures (see Figure 2). TPyP porphyrin was prepared by the condensation of (pyrid-2-yl)benzaldehyde with pyrrole in boiling propionic acid on air [26]. The resulting product was quaternized with methyl tosylate in dimethylformamide (DMF) [27].

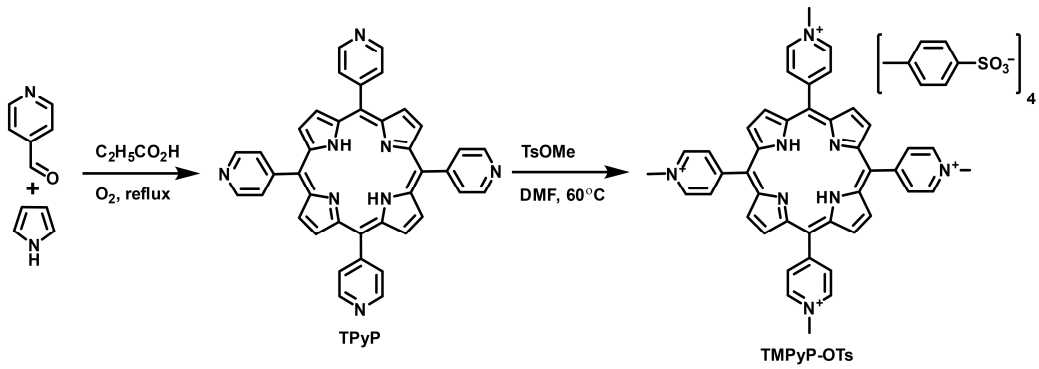

Figure 2. Scheme of TMPyP-OTs porphyrin synthesis.

2.3. Synthesis of Hybrid Nanostructures

Hybrid NPs were obtained by the sequential synthesis. To form hybrid nanostructures, a porphyrin solution was gradually added dropwise into a colloidal solution of gold nanoparticles with continuous stirring. The concentrations of gold nanoparticles and porphyrin were selected in such a way that all the porphyrin from the solution was placed on the surface of the nanoparticles and no free porphyrin remained in the solution. The formation of hybrid structures was controlled by fluorescence spectra shape and by fluorescence quenching in Stern-on-Volmer coordinates. Controlling the shape of the fluorescence spectrum is carried out as follows: in the case of free TMPyP-OTs porphyrin, one broad emission band is observed in the fluorescence spectrum, while two allowed bands are observed during the formation of hybrid nanostructures (Figure 3). The presence of two fluorescence bands is typical for porphyrins, but the porphyrin TMPyP-Ots has a feature that was noted in [28]. The fluorescence spectrum of free porphyrin TMPyP-OTs in a water solution consists of one broad band, while the fluorescence spectrum of porphyrin in hybrid nanostructure composition contains two well-resolved bands. This feature is

associated with the rotation of the pyridinium substituents of free porphyrin, which leads to blurring of the fluorescence bands and merging into one broad band. When porphyrin becomes a part of the hybrid nanostructure, the rotation of the ligands stops and two fluorescence bands are being resolved.

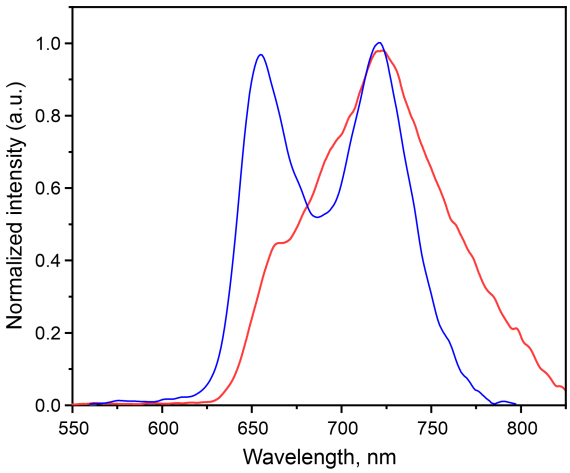

Figure 3. Influence of the porphyrin excess in the water solution of Au NPs and TMPyP-OTs porphyrin on emission spectra, where the red line in a porphyrin excess, the blue line when all porphyrin in the composition of hybrid NPs.

All solutions of hybrid nanostructures were additionally checked for the absence of excess porphyrin not associated with nanoparticles by fluorescence quenching in the Stern–Volmer coordinates, which reflect the dependence of the fluorescence intensity ratio (Io/I) on the quencher concentration (in this case, quencher—gold nanoparticles). The values of Io and I represent the fluorescence intensity of the porphyrin before and after the addition of the quencher, respectively. At the same time, the lifetime of the excited state of porphyrin is measured for all samples. If the lifetime decreases with increasing quencher concentration, then quenching is called dynamic and is determined by the probability of collision between the fluorophore and quencher molecules. If the lifetime of porphyrin in the excited state does not depend on the concentration of the quencher, then such quenching is static and it can be argued that all porphyrin molecules are associated with gold nanoparticles, i.e., hybrid nanostructures are formed.

2.4. Absorption Spectroscopy

The absorption spectra of porphyrins and hybrid nanoparticles aqueous solutions were obtained in the UV-Vis range on the Lambda 1050 spectrophotometer (Perkin Elmer, Glen Waverley, VIC, Australia) equipped with an integrating sphere. The integrating sphere makes it possible to measure the Au NPs and hybrid NPs absorption spectra taking into account the light scattered from the sample. Absorption spectra were measured at 300–800 nm with 1 nm resolution and 1 s per point acquisition time.

2.5. Fluorescence Spectroscopy

The fluorescence spectra and kinetics were carried out on the Fluorolog-3 modular spectrometer (Horiba Scientific). Fluorescence spectra were measured with excitation into the Soret band of porphyrin (420 nm) in a configuration at an angle of 90° in the spectral range 550–780 nm with a 1 mln resolution. A Horiba NanoLED with a radiation wavelength of 390 nm, a pulse duration of 1 ns, and a pulse repetition rate of 80 MHz was used as a pulsed light source for measuring kinetic curves. Kinetic curves were measured by the time-correlated photon counting (TCSPC) method.

The temperature was stabilized using a A28F (Thermo Fisher Scientific, Waltham, MA, USA) water thermostat equipped with Haake SC 100 controller with an accuracy of ±0.1 °C.

3. Results

3.1. Gold Nanoparticles Properties

Colloidal solutions of gold nanoparticles in water were obtained by laser ablation in a liquid using an experimental setup, the optical diagram is shown in Figure 1. Nanoparticles were characterized both in a colloidal solution and when deposited on a substrate. The synthesized Au NPs average diameter about 25 ± 5 nm was determined by the dynamic light scattering method (Figure 4a).

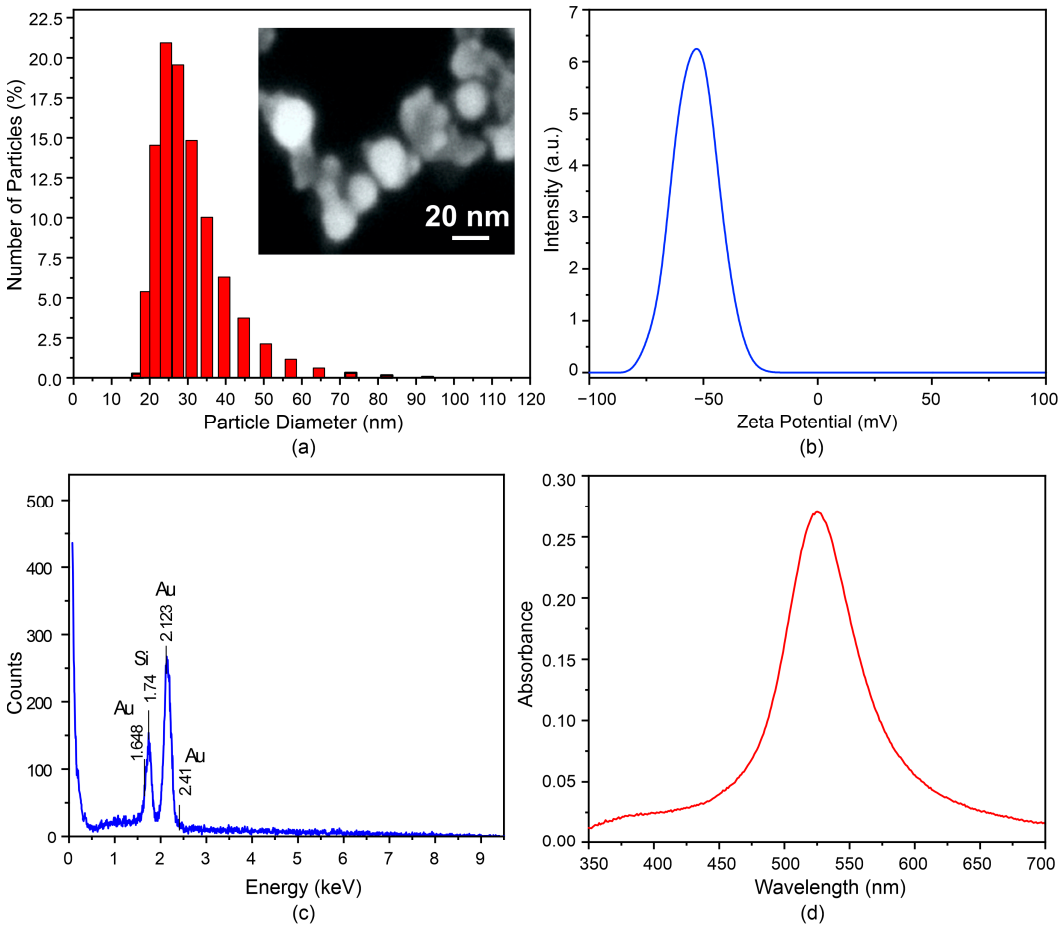

Figure 4. Au NPs size distribution (**a**) in the insert SEM image, Zeta potential (**b**), EDX spectrum (**c**) and absorption spectrum of Au NPs in aqueous solution (**d**).

The statistical data on the size distribution of nanoparticles in the colloidal solution were confirmed by the SEM image of the nanoparticles (inset in Figure 4a). Metal nanoparticles, like bulk metals, are characterized by the presence of a sufficiently large number of free electrons. According to the laws of electrodynamics, free electrons are distributed evenly over the surface of nanoparticles. Thus, while remaining generally electrically neutral, metal nanoparticles have a fairly large negative charge on the surface, which is detected as a negative zeta potential. The colloidal solution of NPs is stable up to a year, which could be highlighted by the rather high value of the Zeta potential at the level of −55 mV (Figure 4b). The high stability of a colloidal solution of gold nanoparticles obtained by laser ablation is determined, first of all, by its high chemical purity. Unlike wet chemistry methods, which are characterized by the presence of reaction byproducts, including ions that form a charged double layer at the surface of nanoparticles, the resulting solutions contain no components

besides purified water and gold. The zeta potential of the resulting nanoparticles in water exceeds −50 mV, which results in effective repulsion of nanoparticles from each other due to Coulomb interaction. Figure 4c shows the results of EDX analysis of gold nanoparticles deposited on a silicon substrate. It is obvious that there are no additional bands other than Au and Si in this spectrum.

The absorption spectrum of Au NPs in water is shown in Figure 4d. The band at 525 nm corresponds to the Au NPs surface plasmon absorption. The relatively small half-width of the band confirms the rather narrow size distribution of particles, and the position of the band agrees with the literature data and correlates with the nanoparticles diameter [5].

3.2. Hybrid Molecular-Plasmon Nanostructures Formation

In order to create hybrid molecular-plasmon nanostructures, a TMPyP-OTs porphyrin was mixed with Au NPs in water. The water solubility of porphyrin is ensured by its ligand environment. In the case of porphyrin TMPyP-Ots the solubility is provided by amino groups, which positive charge is compensated by the SO_3^- anion, leading to the electrical neutrality of the molecules in solution. During the formation of the hybrid structure, the SO_3^- anion is split off and the porphyrin in cationic form is electrostatically attached to the surface of the gold nanoparticle.

The formation of hybrid nanostructures based on gold nanoparticles and porphyrin was controlled by the shape of the fluorescence spectra. Figure 5a shows the fluorescence spectra of an aqueous solution of TMPyP-Ots porphyrin without gold nanoparticles and in the presence of gold nanoparticles. It can be seen that in the concentration range of gold nanoparticles from 4.5×10^{-10} M to 14.6×10^{-10} M, porphyrin with a concentration of 4.6×10^{-8} M hybrid nanostructures are formed. It should be noted that gold nanoparticles reduce the probability of porphyrin radiative transition, as evidenced by the linear dependence of the porphyrin relative emission intensity on the concentration of gold nanoparticles (Figure 5b, red line). On the other hand, the lifetime of the excited state of porphyrin does not depend on the concentration of gold nanoparticles, which indicates static quenching of fluorescence, confirming the formation of hybrid nanostructures.

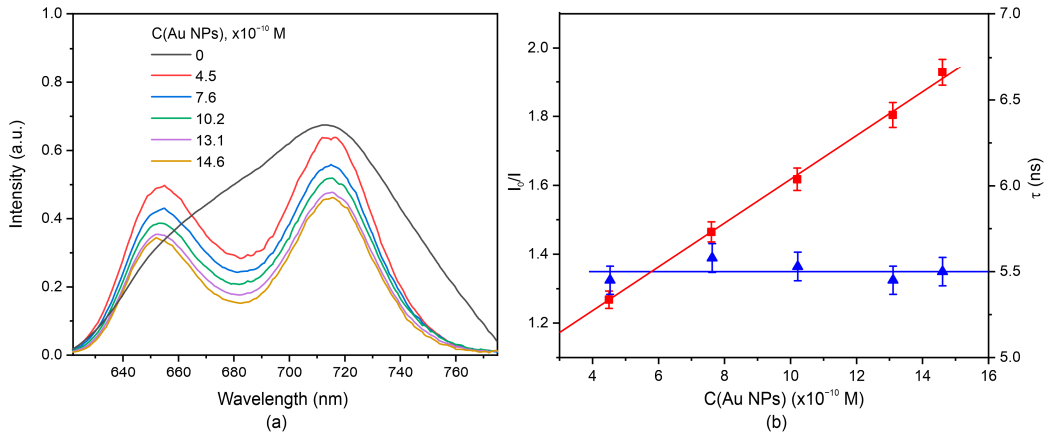

Figure 5. Effect of the concentration of gold nanoparticles on the fluorescence spectra of TMPyP-OTs porphyrin (**a**), relative intensity (red line) and lifetime (blue line) of TMPyP-Ots porphyrin fluorescence in Stern–Volmer coordinates (**b**).

3.3. Properties of Hybrid Molecular-Plasmon Nanostructures Gold Nanoparticles/Porphyrin

The absorption spectra of porphyrin and different concentration of the Au NPs mixture showed the expected increase in the plasmon absorption band accompanied by the rise of the gold concentration (Figure 6a). In addition, the absorption spectra show a Soret band in the 420 nm region and four Q bands in the region of 520, 560, 585 and 650 nm, which

are typical for nonmetallated porphyrins. The corresponding transitions upon optical excitation are shown in the energy level diagram (Figure 6b).

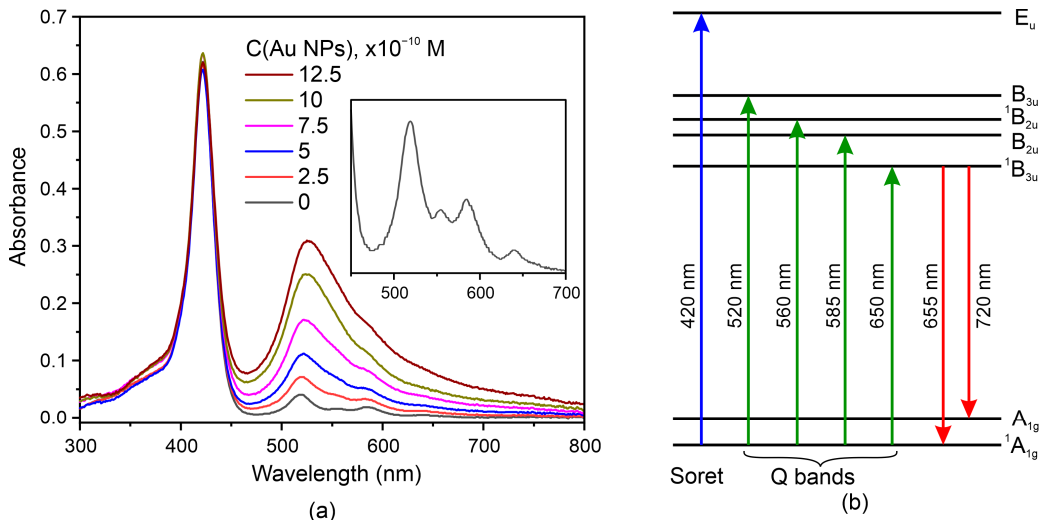

Figure 6. Absorption spectra (**a**) and energy diagram (**b**) of molecular-plasmon systems based on porphyrin and Au NPs with various concentration. Inset Q shows a magnified view of the porphyrin bands.

3.4. Functional Properties of Hybrid Nanostructures Associated with Optical Heating and Fluorescence Thermometry

Heating of molecular-plasmonic hybrid NPs led to a decrease in the radiation intensity with an increasing temperature and a change in the ratio of radiation maxima (Figure 7a). During this experiment, heating was carried out using a thermostat, which stabilized the cuvette temperature for 15 min and maintained it with an accuracy of 0.1 °C at each measured temperature point. The dependence of the fluorescence intensity ratio (FIR) on temperature at a constant porphyrin concentration decreases exponentially (Figure 7b). The statistical deviation does not exceed 1%. This exponential curve is a calibration graph, which can be used to measure the temperature of Au NPs by the ratiometric method.

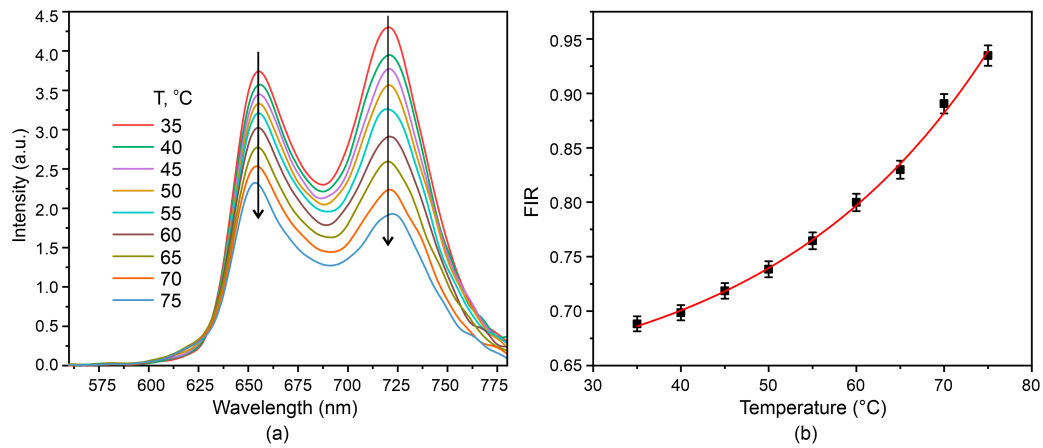

Figure 7. The temperature dependence of hybrid NPs emission spectra under 532 nm excitation (**a**); calibration curve (**b**).

The relative sensitivity S_R and temperature resolution ΔT of fluorescence thermometers in the hybrid NPs was calculated according to equations [29]:

$$S_R = \left| \frac{1}{Q} \frac{\partial Q}{\partial T} \right|, \quad (1)$$

$$\Delta T = \frac{1}{S_R}\frac{\delta Q}{Q}, \tag{2}$$

where Q—temperature parameter (in our case—FIR), T—temperature, $\frac{\delta Q}{Q}$—relative uncertainty. The fluorescence thermometers' relative sensitivity approximately 0.6% and the temperature resolution approximately 0.5 °C for $T = 40$ °C were obtained for developed hybrid NPs.

To demonstrate the operation of porphyrin as a fluorescent thermometer in the molecular plasmon structures composition, the temperature dependence of Au NPs on the laser power was studied. At first, the system fluorescence spectra under different laser power excitation with the subsequent dependence of the peak intensity ratio on the laser power were obtained. Then, based on the calibration curve (Figure 7b), the correlation between the laser excitation power, the relative intensity of the porphyrin emission, and the temperature of the hybrid NPs was determined (Figure 8a), the resulting curve has an exponential character.

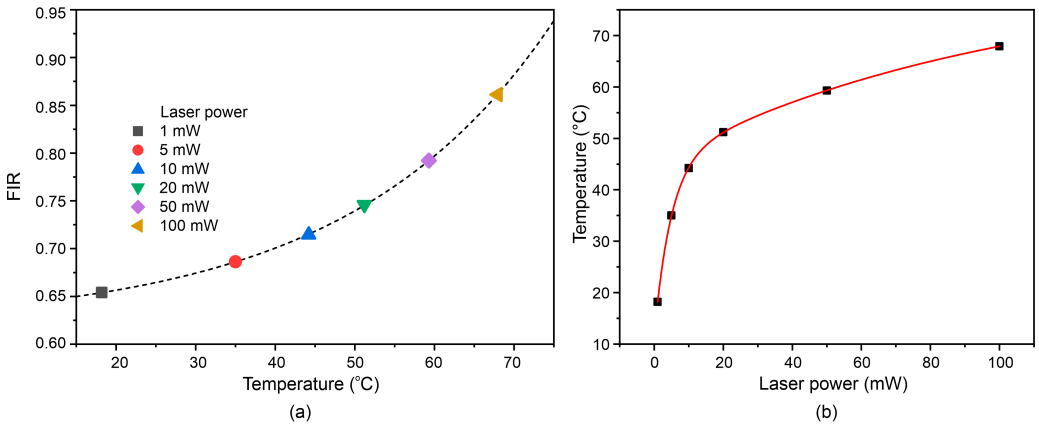

Figure 8. The calibration curve (**a**) and dependence of hybrid NPs in water solution on excitation laser power (**b**).

According to Figure 8b, in order to increase the efficiency of photothermal therapy and reduce the contribution of necrosis to the process of cell death, it is necessary and sufficient to maintain the laser power in the 10–15 mW range. As a result, the photothermal therapy method could be implemented to a new level.

4. Discussion

Hybrid molecular-plasmon NPs were synthesized based on a colloidal solution of Au NPs and water-soluble porphyrin TMPyP-OTs. Au NPs were synthesized by laser ablation of a metal target in water. The obtained colloidal solution of Au NPs is highly stable due to the rather high value of the Zeta potential in the −55 mV region. The NPs diameter is about 25 ± 5 nm, whereas the colloidal solution plasmon absorption band maxima is 525 nm. The obtained characteristics of the synthesized gold nanoparticles are typical for spherical gold plasmonic nanostructures [30]. It should be noted that the synthesized colloidal solutions of gold nanoparticles in water demonstrate high chemical purity, evidenced by no by-products in the reactor except for deionized water and metallic gold. The absence of reaction by-products inherent in wet chemistry methods eliminates the need to clean the surface of nanoparticles. The gold nanoparticles obtained in this work are ready for the formation of hybrid nanostructures without any additional operations.

In the considered system, there are no significant changes in the absorption of porphyrin, in particular, the shift of the Soret band. It can be concluded that the bond between the Au NPs and porphyrins is not very strong, which is explained by the absence of linker ligands. Thus, hybrid nanostructures are formed due to the Coulomb interaction. In this case, the cationic porphyrin is electrostatically retained on the gold surface.

During the formation of the hybrid nanostructure, the porphyrin was attached to the surface of the Au NPs. It was shown that the shape of the porphyrin fluorescence spectrum changes during the hybrid NPs formation compared to the porphyrin solution without Au NPs. This difference was taken as a criterion for the absence of an excess of porphyrin in solution, while a part of the porphyrin is not associated with Au NPs.

The fluorescence spectrum of the nanoparticle/porphyrin hybrid structure differs from the fluorescence spectrum of a solution with a porphyrin excess (Figure 5a). The spectrum shape of the system with an excess of the molecular component corresponds to the fluorescence of free porphyrin. The low resolution of the porphyrin bands could be explained in terms of two approaches. According to the first approach, pyridinium substituents actively rotate upon excitation in an aqueous solution, leading to vibrations in the plane of the common π-electron system of the molecule. These fluctuations result in a decrease in the fluorescence spectrum resolution [28]. The second approach states that porphyrin in an aqueous solution is prone to hydrogen bond formation between the proton of water and the nitrogen of the pyridinium group, leading to energy dissipation due to nonradiative relaxation, which also affects the shape of the fluorescence spectrum. The attachment of a porphyrin molecule to Au NPs takes place due to pyridinium groups, therefore, preventing their rotation and, as a result, fluorescence bands are resolved. In addition, the bond of positively charged nitrogen to a metal surface is stronger than hydrogen bonds. Thus, both approaches can explain the increase in the resolution of fluorescence bands upon binding of free porphyrin to the surface of Au NPs, i.e., the process of hybrid NPs formation. This is also confirmed by the statistical mechanism of quenching of porphyrin TMPyP-Ots fluorescence by gold nanoparticles in hybrid nanostructures. The main confirmation of static quenching is the independence of the TMPyP-Ots porphyrin excited state lifetime from the concentration of gold nanoparticles acting as a quencher. This is only possible in the case of a bound state between the fluorophore and the quencher.

Thus, after the formation of hybrid molecular-plasmon NPs, two well-resolved bands are observed in the fluorescence spectrum of porphyrin, which correspond to the radiative relaxation of the porphyrin from one electronically excited level to two ground levels (Figure 6b). The energy gap between these vibrational sublevels is small; therefore, as the temperature changes, the probability of radiative transitions of the two observed bands changes due to the thermal population of the upper sublevel. This effect is used to create ratiometric fluorescent thermometers based on porphyrins.

The obtained hybrid NPs can be used as photothermal agents for oncological diseases' photothermal therapy. In this case, the porphyrin will act not only as a stabilizing shell, but also as a non-invasive fluorescent thermometer. Such a hybrid system will allow the therapy itself to be carried out by heating plasmonic NPs and, in parallel, to control the heating temperature in order to prevent necrosis. The temperature dependences of a molecular-plasmon system based on porphyrin fluorescence were obtained. The good solubility of the porphyrin in water is an advantage for the in vivo application.

The temperature dependence of the porphyrin fluorescence bands on the composition of hybrid NPs has been investigated. Based on the obtained data, a calibration curve for the dependence of the fluorescence bands integral intensity ratio on temperature was plotted. The fluorescence thermometers relative sensitivity was found to be about 0.6% and 0.5 °C temperature resolution for $T = 40$ °C of hybrid NPs. For fluorescent ratiometric thermometers based on organic phosphors such values of sensitivity and temperature resolution are on the same level as promising organic fluorescent thermometers [31,32].

Using a calibration curve, the possibility of simultaneous heating Au NPs and measuring the temperature with porphyrin under laser excitation was shown. According to the obtained data, the developed hybrid NPs could be considered as a promising material for photothermal therapy.

In presented work, for the first time, the possibility of precision measurement of the temperature of the nanoheaters themselves, and not of the medium they heat was proposed and experimentally confirmed. Thus, the molecular-plasmon system based on Au NPs and

porphyrins is the most promising tool for use in various fields, for example, photothermal therapy, as a parallel thermal agent and molecular fluorescent thermometer. The advantage of the proposed system is a low error in the result determination, a wide range of operation, as well as good solubility and high stability in water.

Author Contributions: Writing—original draft, O.S.S., D.A.S. and A.V.P. (Alexey V. Povolotskiy); Writing—review and editing, A.V.P. (Anastasia V. Povolotckaia) and D.A.L.; Investigation, O.S.S., D.A.L. and A.V.P. (Alexey V. Povolotskiy); Visualization, D.A.S. and A.V.P. (Alexey V. Povolotskiy); Supervision, A.V.P. (Alexey V. Povolotskiy). All authors have read and agreed to the published version of the manuscript.

Funding: This research was funded by RSF grant #23-22-00202.

Data Availability Statement: The data required to reproduce the findings reported in the present work are available in the diagrams, tables, and images of this manuscript.

Acknowledgments: Optical investigations were carried out with equipment of the Laboratory of plasmon-enhanced spectroscopy and bioimaging and Center for Optical and Laser Materials Research, Research Park of Saint-Petersburg State University. SEM and EDX were measured in Interdisciplinary Resource Centre for Nanotechnology, Research Park of Saint-Petersburg State University.

Conflicts of Interest: The authors declare no conflict of interest.

References

1. Luo, D.; Hong, P.; Wu, C.; Wu, S.; Liu, X. Optical Properties of Ag Nanoparticle Arrays: Near-Field Enhancement and Photo-Thermal Temperature Distribution. *Nanomaterials* **2022**, *12*, 3924. [CrossRef]
2. González-Colsa, J.; Serrera, G.; Saiz, J.M.; Ortiz, D.; González, F.; Bresme, F.; Moreno, F.; Albella, P. Gold nanodoughnut as an outstanding nanoheater for photothermal applications. *Opt. Express* **2022**, *30*, 125. [CrossRef] [PubMed]
3. Freitas, L.F.; Ferreira, A.H.; Thipe, V.C.; Varca, G.H.C.; Lima, C.S.A.; Batista, J.G.S.; Riello, F.N.; Nogueira, K.; Cruz, C.P.C.; Mendes, G.O.A.; et al. The State of the Art of Theranostic Nanomaterials for Lung, Breast, and Prostate Cancers. *Nanomaterials* **2021**, *11*, 2579. [CrossRef] [PubMed]
4. Spreafico, C.; Russo, D.; Degl'Innocenti, R. Laser pyrolysis in papers and patents. *J. Intell. Manuf.* **2022**, *33*, 353–385. [CrossRef]
5. Link, S.; El-Sayed, M.A. Size and Temperature Dependence of the Plasmon Absorption of Colloidal Gold Nanoparticles. *J. Phys. Chem. B* **1999**, *103*, 4212–4217. [CrossRef]
6. Wang, Y.; Gao, Z.; Han, Z.; Liu, Y.; Yang, H.; Akkin, T.; Hogan, C.J.; Bischof, J.C. Aggregation affects optical properties and photothermal heating of gold nanospheres. *Sci. Rep.* **2021**, *11*, 898. [CrossRef]
7. Liu, T.; Guo, C.; Li, W.; Fan, S. Thermal photonics with broken symmetries. *eLight* **2022**, *2*, 25. [CrossRef]
8. Alhujaily, M.; Jabir, M.S.; Nayef, U.M.; Rashid, T.M.; Sulaiman, G.M.; Khalil, K.A.A.; Rahmah, M.I.; Najm, M.A.A.; Jabbar, R.; Jawad, S.F. Au/ZnO Nanocomposites Prepared by Laser Ablation for Enhancement of Antibacterial Activity and Cytotoxic Properties against Cancer Cells. *Metals* **2023**, *13*, 735. [CrossRef]
9. Liu, X.-L.; Wang, J.-H.; Liang, S.; Yang, D.-J.; Nan, F.; Ding, S.-J.; Zhou, L.; Hao, Z.-H.; Wang, Q.-Q. Tuning Plasmon Resonance of Gold Nanostars for Enhancements of Nonlinear Optical Response and Raman Scattering. *J. Phys. Chem. C* **2014**, *118*, 9659–9664. [CrossRef]
10. Gautam, A.; Komal, P.; Gautam, P.; Sharma, A.; Kumar, N.; Jung, J.P. Recent Trends in Noble Metal Nanoparticles for Colorimetric Chemical Sensing and Micro-Electronic Packaging Applications. *Metals* **2021**, *11*, 329. [CrossRef]
11. Tanaka, D.; Inuta, Y.; Sakamoto, M.; Furube, A.; Haruta, M.; So, Y.-G.; Kimoto, K.; Hamada, I.; Teranishi, T. Strongest π–metal orbital coupling in a porphyrin/gold cluster system. *Chem. Sci.* **2014**, *5*, 2007–2010. [CrossRef]
12. Shaikh, A.J.; Rabbani, F.; Sherazi, T.A.; Iqbal, Z.; Mir, S.; Shahzad, S.A. Binding Strength of Porphyrin−Gold Nanoparticle Hybrids Based on Number and Type of Linker Moieties and a Simple Method To Calculate Inner Filter Effects of Gold Nanoparticles Using Fluorescence Spectroscopy. *J. Phys. Chem. A* **2015**, *119*, 1108–1116. [CrossRef] [PubMed]
13. Paolesse, R.; Nardis, S.; Monti, D.; Stefanelli, M.; Di Natale, C. Porphyrinoids for Chemical Sensor Applications. *Chem. Rev.* **2017**, *117*, 2517–2583. [CrossRef] [PubMed]
14. Shi, Y.; Zhang, F.; Linhardt, R.J. Porphyrin-based compounds and their applications in materials and medicine. *Dye. Pigment.* **2021**, *188*, 109136. [CrossRef]
15. Huang, W.-B.; Gu, W.; Huang, H.-X.; Wang, J.-B.; Shen, W.-X.; Lv, Y.-Y.; Shen, J. A porphyrin-based fluorescent probe for optical detection of toxic Cd^{2+} ion in aqueous solution and living cells. *Dye. Pigment.* **2017**, *143*, 427–435. [CrossRef]
16. Tsolekile, N.; Nelana, S.; Oluwafemi, O.S. Porphyrin as Diagnostic and Therapeutic Agent. *Molecules* **2019**, *24*, 2669. [CrossRef]
17. Ostovan, A.; Papior, N.; Naghavi, S.S. Half-metallic porphyrin-based molecular junctions for spintronic applications. *Phys. Rev. B* **2021**, *104*, 235435. [CrossRef]

18. Ding, Y.; Zhu, W.-H.; Xie, Y. Development of Ion Chemosensors Based on Porphyrin Analogues. *Chem. Rev.* **2017**, *117*, 2203–2256. [CrossRef] [PubMed]
19. Huang, H.; Song, W.; Rieffel, J.; Lovell, J.F. Emerging applications of porphyrins in photomedicine. *Front. Phys.* **2015**, *3*, 23. [CrossRef]
20. Povolotskiy, A.; Evdokimova, M.; Konev, A.; Kolesnikov, I.; Povolotckaia, A.; Kalinichev, A. Molecular-Plasmon Nanostructures for Biomedical Application. In *Progress in Photon Science*; Springer: Berlin/Heidelberg, Germany, 2019; pp. 173–193.
21. Lupton, J.M. A molecular thermometer based on long-lived emission from platinum octaethyl porphyrin. *Appl. Phys. Lett.* **2002**, *81*, 2478–2480. [CrossRef]
22. Pinto, A.; Pocard, M. Photodynamic therapy and photothermal therapy for the treatment of peritoneal metastasis: A systematic review. *Pleura Peritoneum* **2018**, *3*, 20180124. [CrossRef] [PubMed]
23. Vines, J.B.; Yoon, J.-H.; Ryu, N.-E.; Lim, D.-J.; Park, H. Gold Nanoparticles for Photothermal Cancer Therapy. *Front. Chem.* **2019**, *7*, 167. [CrossRef] [PubMed]
24. Dickerson, E.B.; Dreaden, E.C.; Huang, X.; El-Sayed, I.H.; Chu, H.; Pushpanketh, S.; McDonald, J.F.; El-Sayed, M.A. Gold nanorod assisted near-infrared plasmonic photothermal therapy (PPTT) of squamous cell carcinoma in mice. *Cancer Lett.* **2008**, *269*, 57–66. [CrossRef] [PubMed]
25. Zhang, Y.; Zhan, X.; Xiong, J.; Peng, S.; Huang, W.; Joshi, R.; Cai, Y.; Liu, Y.; Li, R.; Yuan, K.; et al. Temperature-dependent cell death patterns induced by functionalized gold nanoparticle photothermal therapy in melanoma cells. *Sci. Rep.* **2018**, *8*, 8720. [CrossRef] [PubMed]
26. Romera, C.; Sabater, L.; Garofalo, A.; Dixon, I.; Pratviel, G. Interaction of Cationic Nickel and Manganese Porphyrins with the Minor Groove of DNA. *Inorg. Chem.* **2010**, *49*, 8558–8567. [CrossRef]
27. Schulz, S.; Ziganshyna, S.; Lippmann, N.; Glass, S.; Eulenburg, V.; Habermann, N.; Schwarz, U.T.; Voigt, A.; Heilmann, C.; Rüffer, T.; et al. The Meta-Substituted Isomer of TMPyP Enables More Effective Photodynamic Bacterial Inactivation than Para-TMPyP In Vitro. *Microorganisms* **2022**, *10*, 858. [CrossRef]
28. Ou, Z.; Yao, H.; Kimura, K. Organic Nanoparticles of Porphyrin without Self-aggregation. *Chem. Lett.* **2006**, *35*, 782–783. [CrossRef]
29. Dramićanin, M.D. Sensing temperature via downshifting emissions of lanthanide-doped metal oxides and salts. A review. *Methods Appl. Fluoresc.* **2016**, *4*, 042001. [CrossRef] [PubMed]
30. Chen, H.; Kou, X.; Yang, Z.; Ni, W.; Wang, J. Shape- and Size-Dependent Refractive Index Sensitivity of Gold Nanoparticles. *Langmuir* **2008**, *24*, 5233–5237. [CrossRef] [PubMed]
31. Jiang, X.; Dong, Z.; Miao, X.; Wang, K.; Yao, F.; Gao, Z.; Mi, B.; Yi, Y.; Yang, G.; Qian, Y. Fabrication of Flexible High-Temperature Film Thermometers and Heat-Resistant OLEDs Using Novel Hot Exciton Organic Fluorophores. *Adv. Funct. Mater.* **2022**, *32*, 2205697. [CrossRef]
32. Wang, C.; Zhao, X.; Wu, K.; Lv, S.; Zhu, C. A Ratiometric Organic Fluorescent Nanogel Thermometer for Highly Sensitive Temperature Sensing. *Biosensors* **2022**, *12*, 702. [CrossRef] [PubMed]